

**An Infrared Einstein Ring in
the Gravitational Lens PG 1115+080¹**

C. D. Impey

Steward Observatory, University of Arizona, Tucson, AZ 85721
email: cimpey@as.arizona.edu

E. E. Falco, C. S. Kochanek, J. Lehar, and B. A. McLeod

Harvard-Smithsonian Center for Astrophysics, 60 Garden St., Cambridge, MA 02138
email: falco@cfa.harvard.edu, ckochanek@cfa.harvard.edu, jlehar@cfa.harvard.edu,
bmcLeod@cfa.harvard.edu

H.-W. Rix and C. Y. Peng

Steward Observatory, University of Arizona, Tucson, AZ 85721
email: rix@as.arizona.edu, cyp@as.arizona.edu

and

C. R. Keeton

Harvard-Smithsonian Center for Astrophysics, 60 Garden St., Cambridge, MA 02138
email: ckeeton@cfa.harvard.edu

Received _____; accepted _____

Submitted to the *Astrophysical Journal*

¹Based on Observations made with the NASA/ESA Hubble Space Telescope, obtained at the Space Telescope Science Institute, which is operated by AURA, Inc., under NASA contract NAS 5-26555.

ABSTRACT

Hubble Space Telescope observations of the gravitational lens PG 1115+080 in the infrared show the known $z_l = 0.310$ lens galaxy and reveal the $z_s = 1.722$ quasar host galaxy. The main lens galaxy G is a nearly circular (ellipticity $\epsilon < 0.07$) elliptical galaxy with a de Vaucouleurs profile and an effective radius of $R_e = 0''.59 \pm 0''.06$ ($1.7 \pm 0.2h^{-1}$ kpc for $\Omega_0 = 1$ and $h = H_0/100$ km s $^{-1}$ Mpc $^{-1}$). G is part of a group of galaxies that is a required component of all successful lens models. The new quasar and lens positions (3 milliarcsecond errors) yield constraints for these models that are statistically degenerate, but several conclusions are firmly established. (1) The principal lens galaxy is an elliptical galaxy with normal structural properties, lying close to the fundamental plane for its redshift. (2) The potential of the main lens galaxy is nearly round, even when not constrained by the small ellipticity of the light of this galaxy. (3) All models involving two mass distributions place the group component near the luminosity-weighted centroid of the brightest nearby group members. (4) All models predict a time delay ratio $r_{ABC} \simeq 1.3$. (5) Our lens models predict $H_0 = 44 \pm 4$ km s $^{-1}$ Mpc $^{-1}$ if the lens galaxy contains dark matter and has a flat rotation curve, and $H_0 = 65 \pm 5$ km s $^{-1}$ Mpc $^{-1}$ if it has a constant mass-to-light ratio. (6) Any dark halo of the main lens galaxy must be truncated near $1''.5$ ($4h^{-1}$ kpc) before the inferred H_0 rises above ~ 60 km s $^{-1}$ Mpc $^{-1}$. (7) The quasar host galaxy is lensed into an Einstein ring connecting the four quasar images, whose shape is reproduced by the models. Improved NICMOS imaging of the ring could be used to break the degeneracy of the lens models.

Subject headings: quasars – individual: PG 1115+080; H_0 ; gravitational lensing; cosmology

1. INTRODUCTION

Gravitational lens time delays offer a means of determining the Hubble constant that is purely geometrical and hence completely avoids the complications of the local distance scale (Refsdal 1964). The time delay for Q 0957+561 is now well-measured (Schild & Thomson 1997; Kundić et al. 1997; Haarsma et al. 1997), but significant systematic uncertainties remain due to the degeneracy between the mass of the primary lens galaxy and its host cluster (e.g. Grogin & Narayan 1996; Bernstein et al. 1997; Romanowsky & Kochanek 1998). No single lens is likely to be completely free of systematic uncertainties, so a reliable estimate of H_0 should rely on an ensemble of lenses. There are now three more systems with time delay estimates: PG 1115+080 (Schechter et al. 1997), B 1608+656 (Fassnacht et al. 1996), and B 0218+357 (Corbett et al. 1996), which need detailed exploration of their lens models to examine the systematic uncertainties.

PG 1115+080 was the second gravitationally lensed quasar to be discovered (Weymann et al. 1980). The source is an optically selected, radio-quiet quasar at redshift $z_s = 1.722$. Hege et al. (1981) first resolved the four quasar images (a close pair A1/A2, B and C), confirming the early model of Young et al. (1981) that the lens was a five-image system, one image being hidden in the core of the lens galaxy. Henry & Heasley (1986) detected the lens galaxy, followed by gradual improvements in the astrometry by Kristian et al. (1993; hereafter K93), and Courbin et al. (1997). The redshift of the lens galaxy was determined by Angonin-Willaime, Hammer & Rigaut (1993) and confirmed by Kundić et al. (1997) and Tonry (1998) to be $z_l = 0.310$. Tonry also determined the central velocity dispersion of the lens galaxy: $\sigma = 281 \pm 25 \text{ km s}^{-1}$. The spatial resolution of published data has always been insufficient to perform any surface photometry on the lens galaxy. Young et al. (1981) noted that the lens seemed to be part of a small group centered to the southwest of the lens, with a velocity dispersion of approximately $270 \pm 70 \text{ km s}^{-1}$ based on only four galaxy redshifts (Kundić et al. 1997). The group is an essential component of any model that successfully fits the lens constraints (Keeton, Kochanek & Seljak 1997; Schechter et al. 1997). Finally, Schechter et al. (1997) successfully determined two time delays between the images, which were reanalyzed by Barkana (1997) to give $\Delta\tau_{BC} = 25.0_{-1.7}^{+1.5}$ days and the time delay ratio $r_{ABC} = \Delta\tau_{AC}/\Delta\tau_{BA} = 1.13 \pm 0.18$. These results were analyzed by Keeton & Kochanek (1997) and Courbin et al. (1997) to deduce $H_0 = 53_{-7}^{+15} \text{ km s}^{-1} \text{ Mpc}^{-1}$, with comparable contributions to the uncertainties from the time delay measurement and the models. The extreme variations are given in non-parametric form by Saha & Williams (1997), although some of these models may not be physical.

We present new near-infrared observations of the PG 1115+080 system obtained with the Hubble Space Telescope (HST) NICMOS camera. These are the first results of the CfA-Arizona Space Telescope Lens Survey (CASTLES).² After summarizing the

²A summary of gravitational lens data and model results, including CASTLES data, is

observations in §2, we present improved astrometry in §2.1, the first surface photometry of the lens galaxy in §2.2, a discussion of lens models and the Hubble constant in §2.3, photometry of the nearby group in §2.4, and comments on the quasar host galaxy in §2.5. In §3 we comment on the strengths and limitations of this system as a cosmological tool.

2. RESULTS

The HST observations were made on 17 November 1997 using NICMOS Camera 2 and the H (F160W) filter. Four images were taken in a spiral dither pattern for a total integration time of 2560 seconds. The field of view is $\sim 19'' \times 19''$. We reduced the data with a modified pipeline (McLeod 1998). Figure 1a shows the sum of the dithered, flat-fielded F160W images, and Figure 1b shows the image after the quasar point sources were fitted and subtracted. Figures 1c and 1d show model results that are discussed below.

We also reanalyzed the WFPC1 images of K93 from 3 March 1991, which consisted of a 60 second V (F555W) exposure and two 400 second I (F785LP) exposures, and also a deeper set of unpublished WFPC1 images by Westphal (obtained from the STScI archives; hereafter W93) taken on 18 February 1993 and consisting of a total exposure of 4400 seconds in the F555W filter and 7200 seconds in the F785LP filter. The field of view of the images is $\sim 35'' \times 35''$. Figure 2 shows the combined W93 F785LP image scaled to reveal the galaxies making up the surrounding group at the expense of showing the lens geometry.

2.1. Astrometry

We obtained relative astrometry for the quasar images and the lens galaxy using both detailed model fitting (with two independent implementations) and centroiding. The various estimates for the component positions relative to quasar image C in the NICMOS image are consistent to an rms internal measurement error of 2 milliarcseconds (mas), consistent with the variations found by bootstrap error estimation using random combinations of the four NICMOS exposures. The uncertainties are dominated by the effects of binning the images into the approximately 76 mas (two-times oversampled at 38 mas) pixels. We also fitted both the K93 images and the unpublished W93 images. Our fits to the K93 data differ significantly from those in K93, but they are consistent with our fits to the W93 images. The astrometry is listed in Table 1.

The most general global coordinate transformation between the systems is of the form

available at the URL <http://cfa-www.harvard.edu/castles>.

$$T = (1 - \kappa) \begin{pmatrix} \cos \theta & -\sin \theta \\ \sin \theta & \cos \theta \end{pmatrix} + \gamma \begin{pmatrix} \cos 2\theta_\gamma & \sin 2\theta_\gamma \\ \sin 2\theta_\gamma & -\cos 2\theta_\gamma \end{pmatrix} \quad (1)$$

where $1 - \kappa$ represents a scale change, θ represents a global rotation, and γ and θ_γ represent a relative shearing of the coordinates. We have written the transformation in a form that closely corresponds to terms that appear in the gravitational lens constraint equations (e.g., Schneider, Ehlers & Falco 1992). The scale change term is equivalent to adding a convergence κ between the two solutions; it will produce absolute fractional changes in the model parameters and inferred Hubble constant equal to κ . Global rotations will have no effect on the solutions because we have no constraints that depend on the absolute orientation. Coordinate shears are roughly equivalent to the effects of tidal gravity and ellipticity but alter the solutions in a non-trivial way. Fits of the transformation matrix demonstrated that the differences between the astrometric solutions in Table 1 were overwhelmingly dominated by a scale change and a rotation rather than a shear or random errors.

For the astrometric results in Table 1, we adopted pixel scales of $0''.076030$ in the X direction and $0''.075344$ in the Y direction for the NIC2 camera (Cox et al. 1997; from the measurement closest in time to our observations). For the WFPC1 data of Westphal, we adopted the pixel scale of $0''.04404$ from the image headers. Note that this value differs both from the Gould & Yanny (1994) scale of $0''.04374$ and the older calibration of $0''.04389$ used by K93. For these latter two pixel scales, the NICMOS and WFPC1 astrometry differed at the level of 20 mas, which was far larger than any plausible source of errors (Gilmozzi et al. 1995).

With the adopted WFPC1 pixel scale of $0''.04404$, the rms difference between the W93 and NICMOS astrometry is 6 mas. If we allow a small rotation of $\theta \approx 0^\circ.1$ between the images due to the uncertainties in the absolute orientation of the images ($0^\circ.03$ to $0^\circ.05$ rms, see Lupie et al. 1997), the rms differences are only 5 mas. If in addition we allow a small scale difference of $\kappa \simeq 0.0032$, the rms differences are only 1 mas. We finally adopted for our models an uncertainty of 3 mas per coordinate, or slightly over 4 mas per relative coordinate, corresponding to roughly twice the random errors and four times the systematic errors. We also checked the NICMOS astrometry by comparing our position estimates for MG 0414+0534 to VLBI positions (using component b of Trotter 1998), and by comparing our position estimates for H 1413+117 to the ground based astrometry of Schechter (private communication), and in both cases found consistent results at the ≤ 3 mas level.

2.2. Photometry

Table 2 summarizes the photometry for all observations that could reliably detect the lens galaxy. The NICMOS photometry was obtained by fitting a model to the image

using synthetic point-spread functions (PSFs) we generated with Tiny Tim (v4.4; Krist & Hook 1997). We adopt a F160W zeropoint of 1087 Jy for zero magnitudes at an effective wavelength of 1.593 microns, and a conversion rate of 2.77×10^{-6} Jy ADU⁻¹ sec⁻¹. Absolute photometric errors are dominated by the limitations of the PSF model and the zero point uncertainties of about 0.1 mag. The foreground Galactic extinction in the direction of PG 1115+080 is only $E(B - V) = 0.041$ for $R_V = 3.1$ (Schlegel, Finkbeiner & Davis 1998), hence, we applied no corrections to the numbers in Table 2.

The ratios of the quasar fluxes show little variation with wavelength, and most of the observed variations are consistent with the level of temporal variations seen by Schechter et al. (1997). In particular, the curious flux ratio of the close A1/A2 pair is approximately 0.65, independent of wavelength. If we fit the variations with wavelength of the flux ratios with an extinction model using an $R_V = 3.1$ Cardelli et al. (1989) extinction curve in the lens galaxy, we find that the differential extinction between the images is $|\Delta E(B - V)| \lesssim 0.02$ mag and the lens galaxy is virtually dust free. Simple lens models require an A1/A2 flux ratio close to 0.9 because the images are symmetrically arranged near a fold caustic (see Schneider, Ehlers & Falco 1992). Since neither dust nor stellar microlensing is a viable explanation for the observed ratio, we are presumably seeing the effects of a larger perturbation in the gravitational potential produced by a globular cluster or a small satellite galaxy. Images near a caustic (like the A1/A2 pair) are particularly susceptible to magnification perturbations by irregularities of the potential that are too large to produce rapid temporal variations (microlensing) but too small to appreciably alter the image positions or estimates of H_0 (Mao & Schneider 1998).

Our NICMOS observations are the first to resolve the lens galaxy clearly and allow detailed surface photometry models. We fit the lens galaxy as an ellipsoidal de Vaucouleurs model simultaneously with the quasar images using the Tiny Tim PSF model and a constant noise variance. We find a good fit for an effective radius $R_e = 0''.59 \pm 0''.06$, surface brightness $\mu_e = 18.46 \pm 0.20$ H mag arcsec⁻², and an extrapolated total magnitude $m_G = 16.26 \pm 0.05$ H mag. The galaxy model is almost circular with a bound on the axis ratio of $q > 0.93$ (at 1σ , $q > 0.77$ at 3σ), and hence the position angle is unconstrained. For a redshift of 0.31 the effective radius is $1.65 h^{-1}$ kpc ($1.79 h^{-1}$ kpc) for $\Omega_0 = 1$ ($\Omega_0 = 0$). We therefore confirm the lens as a normal elliptical with a luminosity close to L_* .

It is not straightforward to place the lens galaxy on the fundamental plane (FP) for ellipticals because the zero points depend on waveband, redshift, and possibly environment. The most direct comparison can be made with the FP in the cluster Cl1358+62 at $z = 0.33$ (Kelson et al 1997), where no differential K-corrections, or evolutionary corrections are required. We adopt $R_e = 2.36$ kpc (for $q_0 = 0.05$ and $H_0 = 75$ km s⁻¹ Mpc⁻¹), and a rest-frame V band effective surface brightness of $\mu_e(V_{\text{rest}}) = 20.9$, which assumes that $f_\lambda(5500\text{\AA})/f_\lambda(1.2\mu\text{m}) \approx 1.7$ for a 9 Gyr old elliptical of solar luminosity (Vazdekis et al. 1996). Taking $\sigma = 235$ km s⁻¹ from Table 3 (see also §2.3), the lens galaxy in PG1115 has parameters very similar to the FP defined by the galaxies in Cl1358+62: it differs by less

than 0.05 in $\log R_e$ and in $1.24 \log \sigma - 0.33(\mu_e - 25)$.

The lens models discussed in §2.3 determine the mass of the system projected inside the ring radius ($1''.15$) with internal uncertainties of only a few percent. This mass is the sum of the galaxy and group masses, so the mass of the galaxy alone depends on the nature of the group. In models with a singular isothermal sphere (SIS) group, the galaxy mass is $1.24 \times 10^{11} h^{-1} M_\odot$, while in models with a point mass group the galaxy mass is $1.39 \times 10^{11} h^{-1} M_\odot$. We can combine the mass with the photometry to compute a mass-to-light ratio. The galaxy has an H magnitude of 16.60 inside $1''.15$. With models of the spectral evolution of elliptical galaxies we can compute K and evolutionary corrections and transform to rest V or I magnitudes. Unfortunately, different spectral evolution models do not completely agree on the extrapolation. The models of Poggianti (1997) give a V -band magnitude of $M_V = -20.03 + 5 \log h$ (for $\Omega = 1$), while the models of Bruzual & Charlot (1993) give $-20.35 + 5 \log h$. The main difference between the spectral evolution models is the $z = 0$ colors. Poggianti sets the $z = 0$ colors to be the colors of a galaxy at an age of 15 Gyr, while our use of the Bruzual & Charlot models has elliptical galaxies forming at $z = 15$ for a present age of 12.8 Gyr (see Keeton, Kochanek & Falco 1998). The color differences are smaller if we extrapolate only to I band, in which case the Poggianti (Bruzual & Charlot) models give $M_I = -21.46$ (-21.57) $+ 5 \log h$.

The lens models with an SIS group then give I band mass-to-light ratios of $(M/L)_I = 8.2$ (7.4), while the lens models with a point mass group give $(M/L)_I = 9.2$ (8.3). Adopting a $B - I$ color for an old (10 Gyr), solar-metallicity population, these correspond to a more traditional B band mass-to-light ratio of $(M/L)_B = 14.2$ (12.9), and $(M/L)_B = 15.9$ (14.4), respectively. These values are higher than expected from constant mass-to-light stellar dynamical models (e.g. van der Marel 1991), suggesting that we need dark matter, but this conclusion is not robust given the uncertainties in the spectral extrapolation.

2.3. Lens Models and the Hubble Constant

We fitted the quasar and lens galaxy positions, adopting 3 mas uncertainties, and the quasar fluxes (20% uncertainties) using the methods and models of Keeton & Kochanek (1997) and Courbin et al. (1997). We modeled the lens galaxy alternatively as a singular isothermal ellipsoid, an ellipsoidal Hubble law with a core radius of $0''.2$ ($\approx 0.56h^{-1}$ kpc), and an ellipsoidal de Vaucouleurs law combined with a group modeled either as a singular isothermal sphere or a point mass. The de Vaucouleurs model was constrained to match the observed profile of the lens galaxy, with an effective radius $R_e = 0''.6$, ellipticity < 0.07 (1σ), and an unconstrained position angle; in all other models, the ellipticity and position angle were unconstrained. All models led to a well defined group location, a nearly circular lens galaxy even when the ellipticity was unconstrained, and a time delay ratio of

$r_{ABC} \equiv \Delta\tau_{AC}/\Delta\tau_{BA} \simeq 1.3$. The predicted group location is near the luminosity-weighted centroid of the four bright group members (Kundić et al. 1997), and the delay ratio is consistent with the measured $1.13_{-0.17}^{+0.18}$ (Barkana 1997). Figure 3 shows the model group position in relation to the positions of the group galaxies and their centroid. Table 3 lists the parameters of all the variants of our models. Lens positions are not listed because in all models they matched the observed galaxy position within 1 mas. We did not use explicitly the constraints provided by the Einstein ring in our attempts to estimate model parameters, because it is not sufficiently bright. However, we used it to evaluate properties of models constrained by the point images. Figure 1c shows the NICMOS image after the quasar point sources and the lens galaxy have been modeled and subtracted, clearly revealing the Einstein ring due to lensed light from the quasar host galaxy.

All five model families produced acceptable, and statistically indistinguishable, fits to the data, with a $\chi^2 \simeq 3$ (for $N_{dof} = 1$) dominated by the poor fit to the anomalous A1/A2 flux ratio. We note, however, that the variations in χ^2 that yield the parameter errors in Table 3 come equally from all terms and are not dominated by the flux χ^2 . If the lens has dark matter and can be modeled as a singular isothermal ellipsoid, we find $H_0 = 44 \pm 4$ km s⁻¹ Mpc⁻¹; if the lens has a constant mass-to-light ratio, this value increases to $H_0 = 65 \pm 5$ km s⁻¹ Mpc⁻¹. If we use a point mass representation of the group, the value of H_0 rises by approximately 10%. Because the four galaxies are group members, it is plausible that their halos have been tidally stripped to become part of the mean group halo. We fitted the lens using the ellipsoid $\rho \propto 1/r^2(a^2 + r^2)$ where r^2 is the ellipsoidal coordinate, to see how H_0 depends on the halo truncation radius a . Inside a the model has a flat rotation curve and outside a it becomes Keplerian. The model is similar to a Jaffe (1983) model, but its lensing potential is analytic (see Keeton & Kochanek 1998). As expected, the value of H_0 does not change significantly until the truncation radius is comparable to the ring radius, with $H_0 = 47, 49, 53, 56$ km s⁻¹ Mpc⁻¹ for $a = 10'', 5'', 3''$ and $2''$ ($27h^{-1}, 14h^{-1}, 8h^{-1}$ and $5h^{-1}$ kpc for $\Omega_0 = 1$), and we cannot distinguish between the models.

Current evidence indicates that early-type galaxies possess dark matter such that the overall mass profile produces a nearly flat rotation curve. It is found in stellar dynamical models (e.g. Rix et al. 1997), X-ray ellipticals (Fabbiano 1989), and gravitational lensing (Maoz & Rix 1993; Kochanek 1995; Grogin & Narayan 1996). In the case of PG 1115+080, we consider the possibly high mass-to-light ratio as supporting evidence for dark matter associated with the lens. However, a group member may have its halo tidally stripped and merged into the mean group halo. In PG 1115+080, however, the stripping scale for which our models yield $H_0 \geq 65$ km s⁻¹ Mpc⁻¹ is extraordinarily small, particularly since the velocity dispersion of the lens galaxy is comparable to that of the group. Moreover, models of the first lens with a time delay measurement, Q 0957+561, require a nearly isothermal mass distribution on the same scales even though the galaxy is part of a small cluster rather than a small group (Grogin & Narayan 1996).

Note that we quote results only for an $\Omega_0 = 1$ cosmological model. For a low density,

open universe with $\Omega_0 = 0.1$, the Hubble constant would increase by 7.3% and for a flat model dominated by a cosmological constant ($\lambda_0 = 0.8$) the Hubble constant would increase by 4.3%. Fluctuations in the mean line of sight density produced by the non-linear power spectrum of density fluctuations normalized by the local cluster abundance can produce an rms variance of 6% (Seljak 1994; Barkana 1996), with the Hubble constant increasing if there is a void in front of the lens. Most large perturbations produced by the non-linear power spectrum should be positive and associated with visible perturbing objects in the WFPC1 images (e.g., Keeton, Kochanek & Seljak 1997).

2.4. The Nearby Galaxy Group

The galaxy group is an essential component of models for PG 1115+080 (Keeton et al. 1997; Schechter et al. 1997). In fact, some source of additional tidal perturbations appears to be a ubiquitous requirement for good fits to all well-constrained gravitational lenses (Keeton et al. 1997). The roundness of the lens galaxy means that in any constant M/L model the astigmatism of the lens is almost entirely due to the group. Although we neither expect nor observe a strong correlation between the axis ratios of the light and the mass (see Keeton, Kochanek & Falco 1998), even our dark matter models predict that the lens galaxy mass distribution is nearly round.

We have used the unpublished Westphal image to identify 9 new galaxies in the field, within a radius of about $100 h^{-1}$ kpc of the previously known galaxies. Table 4 lists the positions and magnitudes for these new galaxies, along with 3 galaxies that are detected on the NICMOS frame but not with WFPC1. The offsets were determined using the STSDAS task “metric.” Table 4 also includes comments on the morphology, although the aberrated HST images allow no more than a crude characterization of these galaxies. Photometry of the nearby galaxies is obtained using large aperture sizes that include most of their light. No “deblending” was performed for the bright, previously known companions G1, G2, and G3. At $z \approx 0.3$ the sensitivity limit of the WFPC1 data reaches down to objects similar to the LMC, at $M_V \sim -16$. As in the Local Group, there are two luminous spirals (G2 and G3), one of which has two dwarf satellite companions. Most of the other galaxies appear to be early type, although there is one nucleated dwarf. The luminosity weighted centroid of all detected galaxies is $d = 18''.7$ at a position angle of -117° (G12 has been excluded because it may not be a galaxy). This can be compared to $d = 13''.5$ at position angle -115° for the centroid C4 of the main lens galaxy plus G1, G2, and G3. In our refined lens models, the group location in the lens models is well constrained and lies near the centroid C4, with small positional shifts depending on the assumed model (see Figure 3).

With an early-type fraction of 1/3 to 1/2 in this group, we would expect a velocity dispersion in the range 250-400 km s $^{-1}$ (Zabludoff & Mulchaey 1998), consistent with the mass required by the successful lens models and the value measured by Kundić et al. (1997)

of $270 \pm 70 \text{ km s}^{-1}$. Among the isothermal group models, the group has a velocity dispersion ranging from 320 km s^{-1} for the singular isothermal ellipsoidal lens to 430 km s^{-1} for the de Vaucouleurs lens galaxy. The mass inside a cylinder of radius equal to the distance from the group center to the lens galaxy ranges from $2.1h^{-1} \times 10^{12} M_{\odot}$ to $3.5h^{-1} \times 10^{12} M_{\odot}$. The light from the group in the same cylinder is simply the sum of the lens galaxy, G1, G2, and G3 – for a total of $1.7 \times 10^{10} L_{\odot}$ or about $3L_*$. This integral has converged with these four galaxies and does not depend on the group membership of other faint galaxies in the WFPC1 images. We derive a mass-to-light ratio of 40-90 for the *B* band within a radius of $\sim 39h^{-1} \text{ kpc}$, the distance C4-G. These values are consistent with the local estimates for small groups of Ramella, Pisani & Geller (1997), because their estimates used a median radius of $\sim 400 \text{ kpc}$ which would include ten times more mass but no additional light.

2.5. The Quasar Host Galaxy

In addition to the quasar images and the lens galaxy, we also clearly detect an Einstein ring formed by the lensed image of the quasar host galaxy.³ Figure 1c shows the Einstein ring, where residuals remain due to imperfect subtraction of the strong and undersampled quasar images. The flux in the ring is well above the background (10σ to 70σ at a rms noise of $0.001\text{-}0.002 \text{ ADU pixel}^{-1} \text{ sec}^{-1}$). If we break the ring up into polygonal sectors between quasar images A2 and C (#1), C and B (#2), and B and A1 (#3), we find mean *H* band surface brightnesses of $19.43 \pm 0.07 \text{ mag arcsec}^{-2}$ (#1), $20.06 \pm 0.06 \text{ mag arcsec}^{-2}$ (#2), and $18.92 \pm 0.05 \text{ mag arcsec}^{-2}$ (#3). The point source contamination in the aberrated WFPC1 images is too severe to derive a color or a limit on the color of the ring.

We used the lens models fitted in §2.3 to produce models of the ring by adding a lensed exponential disk quasar host galaxy to our photometric model. Figure 1d shows the image that our de Vaucouleurs main lens galaxy and isothermal group would form, after convolution with the appropriate Tiny Tim PSF. The models reproduce the structure of the ring well, but the details of galaxy parameters are sensitive to the large residuals (compared to the ring) created by the mismatch between the model PSF and the quasar images. Detailed modeling of the ring would require a PSF model that matches the observations very accurately. The best fit intrinsic magnitude of the host galaxy is $20.6 H$ mag, compared to $18.7 H$ mag for the quasar, in the SIE/SIS model. Using K-corrections and an evolutionary correction for a passively evolving old stellar population, we compute present-day absolute magnitudes of $M_B = -23.6 + 5 \log h$ ($\Omega = 0.1$) for the quasar and $M_H = -23.4$, i.e. L_* , for the galaxy. Hence, given its host’s luminosity, the quasar is at the maximum luminosity observed in a sample of low-redshift quasars (McLeod & Rieke 1995).

³The ring is also seen in deep WFPC2 I band images (Schechter 1998, private communication).

Since the models fitted to the quasars and the lens galaxy position are degenerate with respect to the value of the Hubble constant, we explored whether improved data on the ring could distinguish between models. The primary difference between the constant M/L and flat rotation curve models lies in the radial magnification profile near the Einstein ring. We took the best fit ring found using the constant M/L galaxy plus SIS group lens model, and then attempted to fit the model ring using the SIE galaxy plus SIS group lens model while adjusting the source galaxy parameters to find the best fit. The largest differences are concentrated near the center of the quasar host galaxy and lie under the quasar images, but significant residuals appear in the regions away from the quasar images. The best-fit source for the SIE model is too broad to fit the “de Vaucouleurs ring” regardless of the host galaxy’s scale length, leaving residuals at the level of ~ 0.01 ADU pixel $^{-1}$ sec $^{-1}$, or a surface brightness of $20.8 H$ mag arcsec $^{-2}$ in the regions away from the quasar images. Hence, images with accurately matched PSFs and with significantly reduced contrast between the quasar and host galaxy images could directly discriminate between lens models of differing radial mass profile.

3. DISCUSSION

New infrared data on PG 1115+080 affirms multiple-component gravitational lens systems as powerful cosmological tools. The major puzzle remaining in the PG 1115+080 system is the anomalous A1/A2 flux ratio. Our observations rule out differential extinction as an explanation, and microlensing is ruled out by its lack of variability. Since a flux ratio near 0.9 is a generic feature of the large scale potential near a fold caustic, only a potential perturbation intermediate between that produced by isolated stars (microlensing) and by the overall galaxy can explain the flux ratio. The potential of PG 1115+080 must be perturbed either by a satellite galaxy or a globular cluster. Mao & Schneider (1998) showed that such perturbations alter the time delay – and so the inferred value of the Hubble constant – fortunately by no more than 2-3%.

Our improved astrometry greatly reduces some of the degeneracies in early models of the system. The group position is now well constrained and located near the luminosity centroid of the four bright group galaxies, and the lens galaxy is constrained to be nearly circular. Unfortunately, the degeneracies in the H_0 estimate have been exacerbated because with the revised astrometry the models no longer favor dark matter models over constant M/L models for the main lens galaxy. Because all 4 images are located at nearly the same radial distance from the center of the lens galaxy, we do not expect the models to be sensitive to the radial mass profile of the lens galaxy (Kochanek 1991; Wambsganss & Paczynski 1994). We find H_0 ranging from 44 ± 4 km s $^{-1}$ Mpc $^{-1}$ if the lens galaxy is modeled as a singular isothermal ellipsoid and the group as a singular isothermal sphere, to 65 ± 5 (72 ± 5) km s $^{-1}$ Mpc $^{-1}$ for $\Omega_0 = 1$ (0.1) if the lens galaxy has a constant M/L . Note that we find evidence for dark matter in our high value of M/L . A model with an

adjustable truncation radius shows that the halo must be truncated on scales comparable to the ring diameter for H_0 to exceed $60 \text{ km s}^{-1} \text{ Mpc}^{-1}$. Such a halo seems smaller than physically plausible given that the velocity dispersions of the group and the lens galaxy are comparable.

Further progress in reducing the uncertainties depends on improving the time delay measurements and on making more detailed studies of the Einstein ring formed by the quasar host galaxy. First, for any given mass profile, most of the current errors in H_0 are due to the uncertainties in the time delays. Second, all the best fit models predict time delay ratios near $r_{ABC} = 1.3$, consistent with the current measurement of 1.13 ± 0.18 . If nothing else, a more accurate measurement of the delay ratio than is now available would be a powerful test of the models. For any given lens mass profile, the ratio constraint would further reduce the parameter space for the position and mass of the group, or could be used to constrain more complicated models (e.g., Saha & Williams 1997). Deep new observations to determine the surface brightness of the ring accurately, combined with direct measurement of the point spread function at the time of the observations would probably permit us directly to break the degeneracy of the models. Only NICMOS, however, has the ability to make these difficult observations within a decade.

No single technique or observation can tie down the Hubble constant – the long history of unrecognized or underestimated systematic errors in this subject encourages humility. Nevertheless, PG 1115+080 demonstrates the potential of the gravitational lens approach. With recent reductions in age estimates of the oldest globular clusters (Chaboyer et al. 1998), and the likelihood that the mass density of the universe is lower than the Einstein-de Sitter case (e.g., Garnavich et al. 1998), the possibility of an age conflict in the big bang model has receded. The modeling of PG 1115+080 gives a plausible upper bound on the Hubble constant if we accept that the group is not a point mass and that the lens galaxy is unlikely to have a mass distribution that is more concentrated than its light distribution. This bound is $H_0 < 67 \text{ (72) km s}^{-1} \text{ Mpc}^{-1}$ for $\Omega_0 = 1 \text{ (0.1)}$. The most recent result of the HST Extragalactic Distance Scale Key Project is $H_0 = 72 \pm 5 \text{ (random)} \pm 12 \text{ (systematic) km s}^{-1} \text{ Mpc}^{-1}$ (Madore et al. 1998). Our upper limit is inconsistent with the upper end of the range from the Key Project, although it is consistent with the lower end of the range. There appears to be satisfactory concordance among the basic parameters of the big bang model, and between direct and indirect measures of the distance scale. Gravitational lenses can be expected to play an increasing role as versatile cosmological tools.

We would like to thank many people in the NICMOS team who provided advice and technical information. In particular, Marcia Rieke and Dean Hines helped with photometry issues and Glenn Schneider, Ray Lucas and the STScI Help Desk helped with astrometric issues. CDI acknowledges support from NSF under grant AST-9320715. CSK

and CRK acknowledge financial support from NASA under ATP grant NAG5-4062, and from NSF under grant AST-9401722. Support for this work was provided by NASA through grant number GO-7495 from the Space Telescope Science Institute, which is operated by the Association of Universities for Research in Astronomy, Inc., under NASA contract NAS5-26555.

REFERENCES

- Angonin-Willaime, M.-C., Hammer, F., & Rigaut, F. 1993, in *Gravitational Lenses in the Universe*, eds. J. Surdej et al. (Universite de Liege: Liege), p. 85
- Barkana, R. 1996, *ApJ*, 468, 17
- Barkana, R. 1997, *ApJ*, 489, 21
- Bernstein, G., Fischer, P., Tyson, J. A. & Rhee, G. 1997, *ApJ*, 483, 79
- Bruzual, G., & Charlot, S. 1993, *ApJ*, 405, 538
- Cardelli, J., Clayton, G. C. & Mathis J. S., *ApJ*, 1989, 345, 245
- Chaboyer, B., Demarque, P., Kernian, P.J., & Krauss, L.M. 1998, *ApJ*, 496, 96
- Christian, C.A., Crabtree, D., & Waddell, P. 1987, *ApJ*, 312, 45
- Corbett, Browne, I.W.A., Wilkinson, P.N., & Patnaik, A.R. 1996, in *Astrophysical Applications of Gravitational Lensing*, eds. C.S. Kochanek and J.N. Hewitt (Kluwer Academic Publishers: Dordrecht), p. 37
- Courbin, F., Magain, P., Keeton, C.R., Kochanek, C.S., Vanderriest, C., Jaunsen, A.O., & Hjorth, J. 1997, *A&A*, 324, L1
- Cox, C., Ritchie, C., Bergeron, E., Mackenty, J., & Noll, K. 1997, *NICMOS Instrument Science Report 97-07*, Space Telescope Science Institute
- Fabbiano, G. 1989, *ARA&A*, 27, 87
- Fassnacht, C.D., Womble, D.S., Neugebauer, G., Browne, I.W.A., Readhead, A.C.S., Matthews, K., & Pearson, T.J. 1996, *ApJ*, 460, 103
- Garnavich, P., M., Schommer, R., Schmidt, B., Jha, S., Challis, P., Filippenko, A.V., Riess, A.G. & Leonard, D.C. 1998, *ApJ*, 493, 53
- Gilmozzi, R., Ewald, S., & Kinney, E. 1995, *WFPC2 Instrument Science Report 95-02*, Space Telescope Science Institute
- Gould, A., & Yanny, B. 1994, *PASP*, 106, 101
- Grogin, N.A., & Narayan, R. 1996, *ApJ*, 464, 92
- Haarsma, D.B., Hewitt, J.N., Lehár, J., & Burke, B.F. 1997, *ApJ*, 479, 102
- Hege, E.K., Hubbard, E.N., Strittmatter, P.A., & Worden, S.P. 1981, *ApJ*, 248, L1

- Henry, J.P., & Heasley, J.N. 1986, *Nature*, 321, 142
- Holtzman, J., Groth, E.J., Light, R.M., Faber, S.M., et al. 1991, *ApJ*, 369, L35
- Jaffe, W. 1983, *MNRAS*, 202, 995
- Jorgensen, I., Franx, M., & Kjaergaard, R. 1996, *MNRAS*, 280, 167
- Keeton, C.R., & Kochanek, C.S. 1997, *ApJ*, 487, 42
- Keeton, C.R. & Kochanek, C.S. 1998, 495, 157
- Keeton, C.R., Kochanek, C.S., & Falco, E. E. 1998, *ApJ* in press (astro-ph/9708161)
- Keeton, C.R., Kochanek, C.S., & Seljak, U. 1997, *ApJ*, 482, 604
- Kelson, D.D., van Dokkum, P.G., Franx, M., Illingworth, G.D., & Fabricant, D. 1997, *ApJ*, 478, L13
- Kochanek, C.S. 1995, *ApJ*, 453, 545
- Krist, J. E. & Hook, R. N. 1997, *The Tiny Tim User's Guide*, version 4.4 (Baltimore: STScI)
- Kristian, J., Groth, E.J., Shaya, E.J., et al. 1993, *AJ*, 106, 1330 (K93)
- Kundić, T., Turner, E.L., Colley, W.N., Gott, J.R. III, Rhoads, J.E., Wang, Y., Bergeron, L.E., Golria, K.A., Long, D.C., Malhotra, S., & Wanbgsanss, J. 1997, *ApJ*, 482, 75
- Kundić, T., Cohen, J.G., Blandford, R.D., & Lubin, L.M. 1997, *AJ*, 114, 507
- Lupie, O., Lallo, M., Cox, C., & Bergreon, E. 1997, *NICMOS Instrument Science Report 97-04*, Space Telescope Science Institute
- Madore, B.F., et al. 1998, *Nature*, in press
- Mao, S., & Schneider, P. 1998, *A&A*, in press
- Maoz, D.. & Rix, H.-W. 1993, *ApJ*, 416, 425
- McLeod, B.A. 1998, in *1997 HST Calibration Workshop*, ed S. Casertano et al., Space Telescope Science Institute, in press
- McLeod, K. K., & Rieke, G. H. 1995, *ApJ*, 454, L77
- Poggianti, B.M. 1997, *A&AS*, 122, 399
- Ramella, M., Pisani, A., & Geller, M.J. *AJ*, 113, 483

- Refsdal, S. 1964, MNRAS, 128, 295
- Rix, H.-W., de Zeeuw, P.T., Cretton, N., van der Marel, R.P., & Carollo, C.M. 1997, ApJ, 488, 702
- Romanowsky, A. & Kochanek, C. S. 1998, ApJ in press (astro-ph/9708212)
- Saha, P. & Williams, L. L. R. 1997, MNRAS, 292, 148
- Schechter, P.L., Bailyn, C.D., Barr, R., et al. 1997, ApJ, 475, L85
- Schild, R.E., & Thomson, D.J. 1997, AJ, 113, 130
- Schlegel, D. J., Finkbeiner, D. P. & Davis, M. 1998, ApJ in press (astro-ph/9710327)
- Schneider, P., Ehlers, J., and Falco, E.E. 1992, Gravitational Lenses (Springer-Verlag: Berlin)
- Seljak, U. 1994, ApJ, 436, 509
- Tonry, J.L. 1998, AJ, 115, 1
- Trotter, C. 1998, Ph.D. Thesis, Massachusetts Institute of Technology
- van der Marel, R.P. 1991, MNRAS, 253, 710
- Vazdekis, A., Casuso, E., Peletier, R., Beckman, J., 1996, ApJS, 106, 307.
- Weymann, R.J., Latham, D., Angel, J.R.P., Green, R.F., Liebert, J.W., Turnshek, D.A., Turnshek, D.E., & Tyson, J.A. 1980, Nature, 285, 641
- Young, P.J., Deverill, R.S., Gunn, J.E., Westphal, J.A., & Kristian, J. 1981, ApJ, 244, 756
- Zabludoff, A.I., & Mulchaey, J.S. 1998, ApJ, in press

Table 1. Astrometry of the PG 1115+080 System.

Image	HST/NICMOS ^a		HST/WFPC1 ^b		HST/WFPC1 ^c		NOT ^d	
	$\Delta(\text{RA})$ ($''$)	$\Delta(\text{Dec})$ ($''$)	$\Delta(\text{RA})$ ($''$)	$\Delta(\text{Dec})$ ($''$)	$\Delta(\text{RA})$ ($''$)	$\Delta(\text{Dec})$ ($''$)	$\Delta(\text{RA})$ ($''$)	$\Delta(\text{Dec})$ ($''$)
A1	+1.328	-2.037	+1.318	-2.032	+1.313	-2.031	+1.291	-2.028
A2	+1.478	-1.576	+1.468	-1.578	+1.463	-1.577	+1.445	-1.578
B	-0.341	-1.960	-0.350	-1.956	-0.346	-1.956	-0.364	-1.940
C	$\equiv 0$	$\equiv 0$	$\equiv 0$	$\equiv 0$	$\equiv 0$	$\equiv 0$	$\equiv 0$	$\equiv 0$
Lens	+0.382	-1.344	+0.386	-1.362	+0.332	-1.339

^aHST/NICMOS F160W image presented in this paper. The rms internal error on each measurement is $0''.002$. Plate scales are $0''.076030$ per pixel in X and $0''.075344$ per pixel in Y with an orientation of $68^\circ 760$.

^bHST/WFPC1 F785LP image W93, previously unpublished. The plate scale is $0''.04404$ with an orientation of $123^\circ 087$.

^cHST/WFPC1 F785LP, new measurements of an image published by Kristian et al. (1993).

^dFor comparison, Nordic Optical Telescope *I* band results of Courbin et al. (1997) using an astrometric solution adapted to positions measured by Kristian et al. (1993).

Table 2. Photometry of the PG 1115+080 System.^a

Image	NICMOS ^b	HST/WFPC1 ^c		HST/WFPC1 ^d		NOT ^e	CFHT ^f		
	<i>H</i> (mag)	<i>I</i> (mag)	<i>V</i> (mag)	<i>I</i> (mag)	<i>V</i> (mag)	<i>I</i> (mag)	<i>R</i> (mag)	<i>V</i> (mag)	<i>B</i> (mag)
A1	15.44±0.02	16.12	16.90	16.19	16.81	16.34	16.71	16.99	17.48
A2	15.92±0.03	16.51	17.35	16.56	17.32	16.75	16.95	17.27	17.74
B	17.37±0.04	18.08	18.87	18.05	18.73	18.30	18.46	18.74	19.19
C	16.92±0.03	17.58	18.37	17.60	18.40	17.82	17.97	18.26	18.71
Lens	16.26±0.10	18.40	...	18.55	...	19.60	20.20	20.90	...

^aMagnitudes are not corrected for the estimated foreground extinction of $E(B - V) = 0.041$ mag estimated by Schlegel, Finkbeiner & Davis (1998).

^bH(F160W) band data from this paper. The zero point is uncertain by 0.1 mag, and the total lens magnitude is from a model fit.

^cI(F785LP) and V(F555W) band data image from Kristian et al. (1993). The zero points are from Holtzman et al. (1991).

^dI(F785LP) and V(F555W) band data image from unpublished W93 image. The zero points are from Holtzman et al. (1991).

^eI band data from Courbin et al. (1997). The lens magnitude is measured in a $0''.9$ aperture, and no zero point error is quoted.

^fBVR band data from Christian et al. (1987). The lens magnitude is measured in a $1''.6$ aperture, with a zero point accurate to 0.05 mag.

Table 3. Lens Model Results

	SIE ^a / SIS	Hub ^b / SIS	de Vauc ^c / SIS	SIE ^a / Pt	Hub ^b / Pt
Galaxy ^d					
b (")	1.04 ± 0.01	1.03 ± 0.01	1.03 ± 0.01	1.15 ± 0.01	1.15 ± 0.01
M ($10^{11}h^{-1}M_{\odot}$)	1.25 ± 0.02	1.24 ± 0.01	1.24 ± 0.01	1.39 ± 0.01	1.38 ± 0.01
σ (km/s)	230 ± 1	—	—	243 ± 1	—
q	0.96 ± 0.03	0.96 ± 0.04	0.96 ± 0.04	0.95 ± 0.02	0.96 ± 0.02
PA (°)	46_{-34}^{+16}	61_{-44}^{+17}	68 ^d	28_{-25}^{+20}	30_{-25}^{+33}
Group ^e					
b (")	2.0 ± 0.4	3.1 ± 0.4	3.6 ± 0.4	4.3 ± 0.7	5.2 ± 0.6
M ($10^{11}h^{-1}M_{\odot}$)	20.8 ± 5.0	34.9 ± 6.7	42.5 ± 7.2	19.7 ± 6.3	27.9 ± 7.0
σ (km/s)	320 ± 32	397 ± 26	428 ± 24	—	—
d_{grp} (")	10.0 ± 1.3	10.8 ± 1.5	11.3 ± 1.3	12.8 ± 1.6	12.6 ± 1.6
θ_{grp} (°)	-113 ± 2	-116 ± 1	-116 ± 1	-112 ± 2	-114 ± 1
H_0 (km s ⁻¹ Mpc ⁻¹)	44 ± 4	61 ± 5	65 ± 5	47 ± 4	68 ± 6
Best-fit Model ^f					
Source $\Delta\alpha$ (")	-1.79	-2.73	-3.16	-1.33	-1.88
Source $\Delta\delta$ (")	-0.69	-1.18	-1.41	-0.44	-0.71
Source Flux	0.17	0.33	0.39	0.20	0.42
Total Magnification	46	24	20	40	19
χ^2 (positions)	0.03	0.05	0.04	0.10	0.05
χ^2 (fluxes)	3.58	3.06	3.06	4.36	4.14
χ^2 (galaxy)	0.02	0.05	0.26	0.12	0.08
χ^2 (total)	3.63	3.16	3.36	4.57	4.27

^aSingular isothermal ellipsoid galaxies with an unconstrained ellipticity and position angle.

^bEllipsoidal Hubble model galaxies with a fixed core radius of $0''.2 = 0.56h^{-1}$ kpc, and an unconstrained ellipticity and position angle.

^cEllipsoidal de Vaucouleurs model galaxies constrained to match the observed profile of the lens galaxy, with an effective radius $R_e = 0''.6$, an ellipticity < 0.07 (1σ), and an unconstrained position angle. The model PA can take any value at the $\Delta\chi^2 = 1$ level.

^dThe best-fit values and $\Delta\chi^2 = 1$ error bars result from the variation of the lens galaxy’s critical radius b , position, axis ratio q , and position angle. No PA error bar is quoted for the de Vaucouleurs galaxy model because the PA can take any value at the $\Delta\chi^2 = 1$ level. The mass M inside the ring radius $1''.15$, and σ for isothermal galaxies is given.

^eWe varied the group critical radius b , and position in polar coordinates (d_{grp}, θ_{grp}) centered on the lens galaxy. We give the mass M inside a cylinder of radius equal to d_{grp} , and the velocity dispersion σ for SIS groups.

^fParameters for the best-fit models, including the source position (relative to the lens galaxy), the source flux (relative to image A_1), the total magnification, and the contribution to the χ^2 from the image positions, the fluxes, and the galaxy position.

Table 4. Nearby Galaxies in the PG 1115+080 Field

Name	F785LP ^a		F555W		F160W ^b		RA ^c	Dec	Comments ^d
	<i>I</i>	$\sigma(I)$	<i>V</i>	$\sigma(V)$	<i>H</i>	$\sigma(H)$	Offset (arcsec)		
	(mag)		(mag)		(mag)				
Lens ^e	18.55	0.50	16.26	0.10	0.382	−1.344	Elliptical, $z = 0.310^f$
G1	17.85	0.01	20.40	0.03	−20.139	−12.347	Sp/S0, $z = 0.310$
G2	18.73	0.04	21.05	0.06	−11.547	−2.167	Sp, face-on, $z = 0.312$
G3	19.44	0.02	21.69	0.07	−13.607	−13.516	Sp, edge-on, $z = 0.309$
G4	19.88	0.04	22.46	0.12	−61.151	−19.406	Sp/S0?
G5	20.63	0.06	−17.588	−40.630	E?
G6	21.38	0.13	−26.196	−31.996	dE?
G7	21.40	0.08	−34.785	−24.919	dIrr?
G8	21.52	0.08	−27.706	−13.546	dE?
G9	22.05	0.27	−13.311	−5.643	dw companion to G2
G10	22.09	0.09	23.56	0.10	−41.203	−3.078	dIrr?
G11	22.98	0.34	−10.957	−4.892	dw companion to G2
G12	18.55	0.08	2.946	−43.246	K93 image (star?)
G13	21.36	0.13	7.934	−4.575	
G14	20.94	0.07	3.494	−7.962	
G15	21.47	0.10	3.108	−13.234	

^aF785LP and F555W data derived from W93 images

^bF160W data from the NICMOS image presented in this paper

^cOffsets are calculated relative to component C of PG 1115+080

^dMorphological information from W93 images, except where otherwise indicated

^eOffset for the lens from our NICMOS image. The magnitude is our own estimate from fitting the point images and a de Vaucouleurs profile to the W93 I-band image

^fAll redshifts are from Kundić et al. (1997)

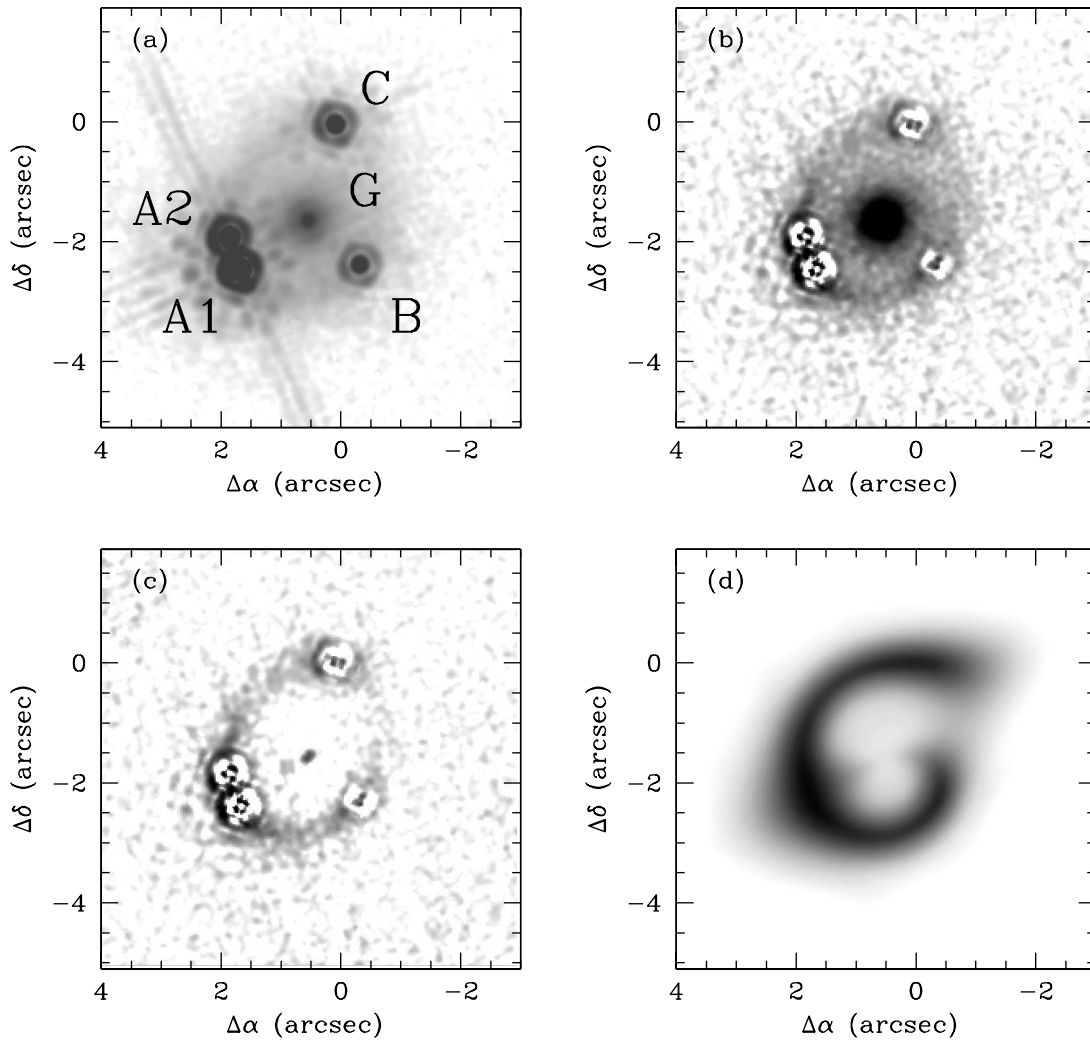


Fig. 1.— NICMOS image of the PG 1115+080 system, taken with Camera 2 and the F160W filter. Each panel is $\sim 7'' \times 7''$, and is oriented with North at the top and East at the left. (a) The sum of the dithered, flat-fielded exposures. The four quasar images are separated by $\sim 1''.3$. (b) The same image after fitting and subtracting quasar point sources. Artifacts remain due to imperfect subtraction of the point spread function. The main lens galaxy is well resolved; an Einstein ring is perceptible. (c) The same image after subtracting the main lens galaxy, modeled as a de Vaucouleurs profile; a nearly complete Einstein ring is now easily visible. (d) The Einstein ring that the de Vaucouleurs + SIS model predicts, after convolution with an appropriate Tiny Tim PSF. Note that the ring is closed: there is very faint flux between images B and C.

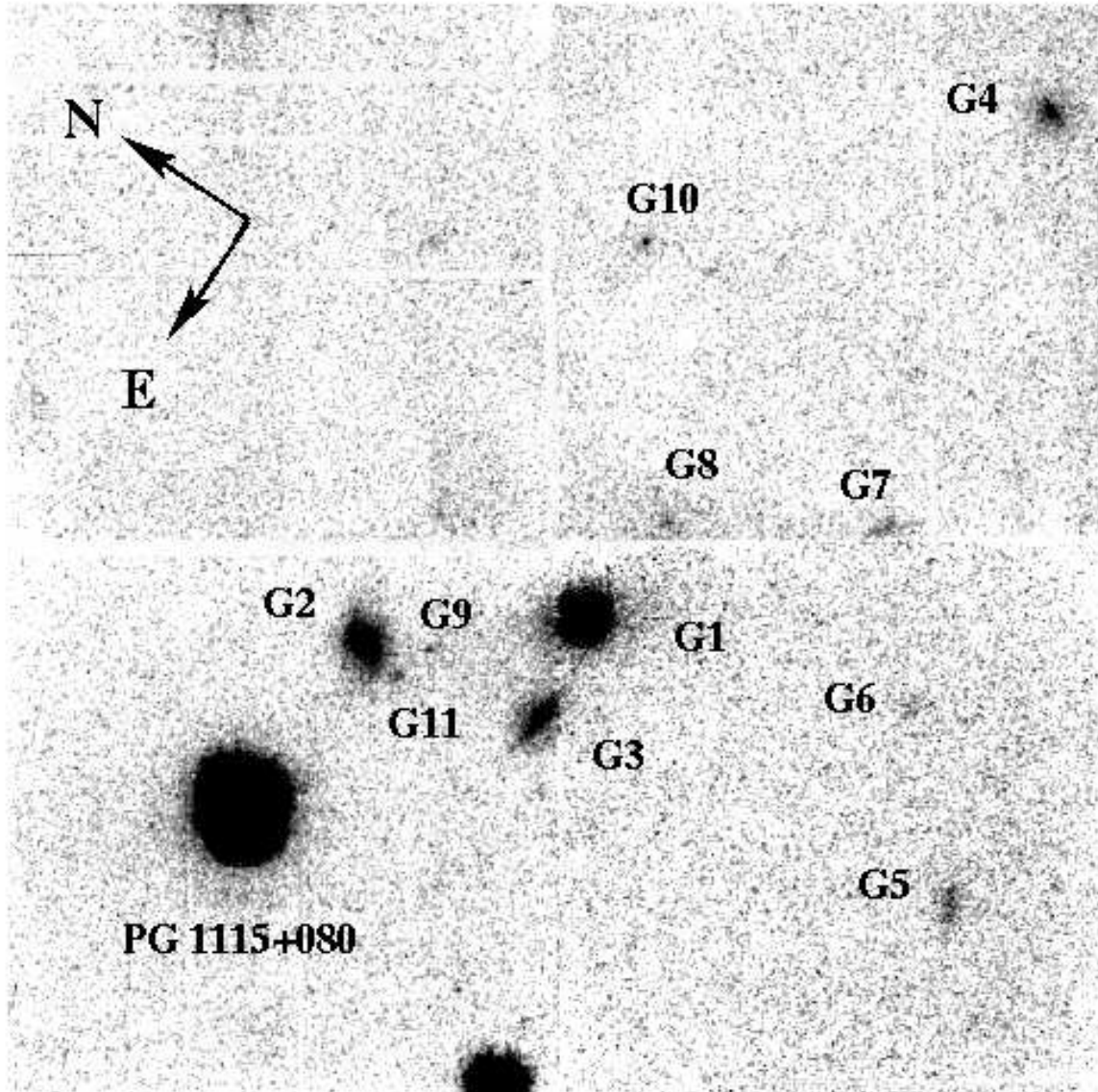


Fig. 2.— Archival WFPC1 image of the PG 1115+080 system (W93), taken through the F785LP filter. We smoothed the image with a gaussian with $\sigma = 2$ pixels, to improve the contrast for the faintest features. The multiply imaged quasar is saturated in this representation. Nine galaxies near the lens system are listed in Table 4, along with 3 galaxies seen only on the NICMOS image. Although part of the bright object at the bottom of the image fell outside the WFPC1 field of view, it clearly appears to be a star.

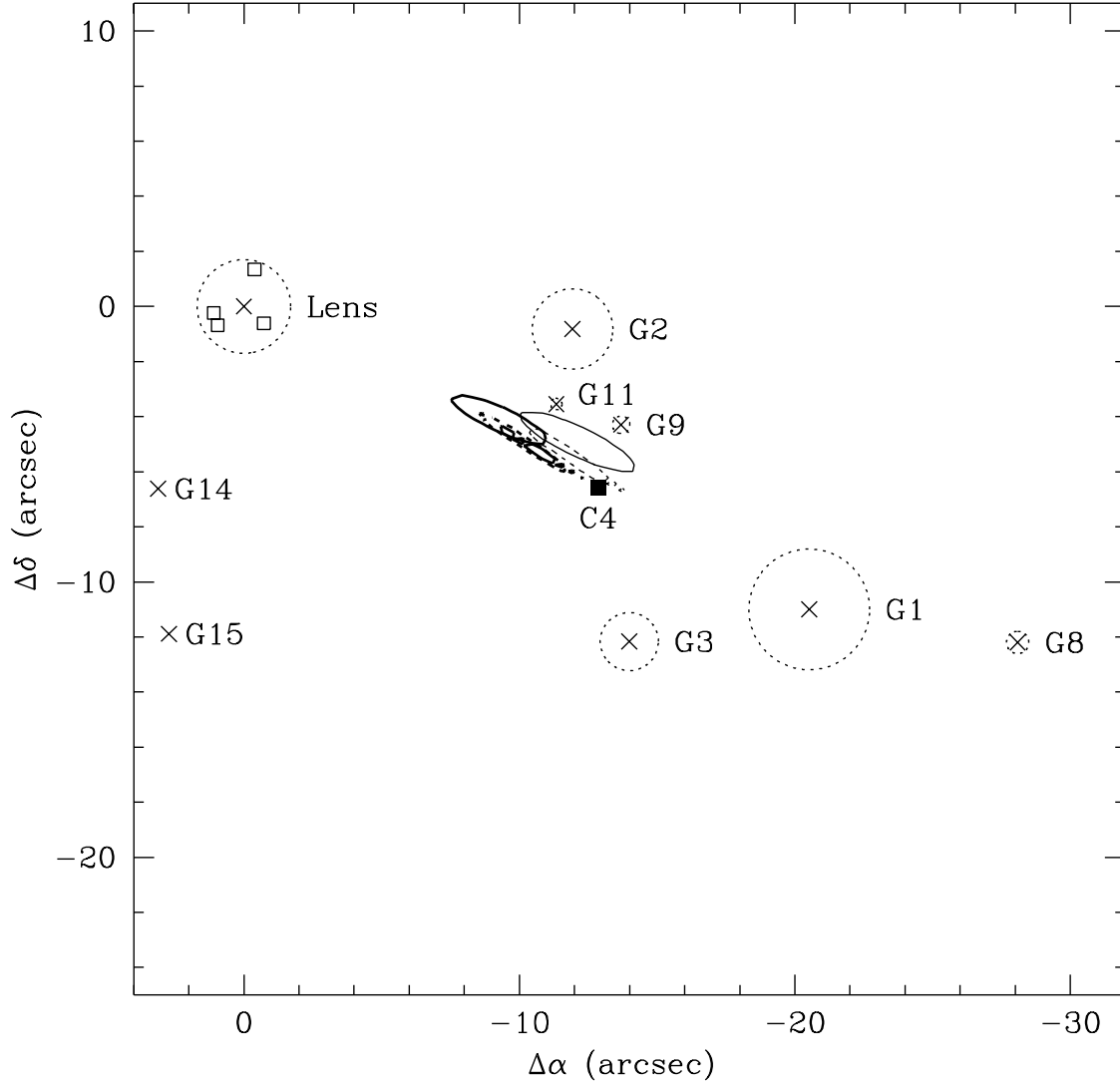


Fig. 3.— The model group positions on the sky, shown as position error ellipses (bold solid: isothermal galaxy + SIS; light solid: isothermal galaxy + point mass; bold dotted: Hubble galaxy + SIS; light dotted: Hubble galaxy + point mass; bold dashed: de Vaucouleurs galaxy + SIS). Also shown are the positions of the lensed images, the main lens galaxy, the group galaxies and the centroid C4 of the main lens galaxy plus G1, G2, and G3. The area of each dotted circle is proportional to the F785LP flux of the corresponding galaxy.